Long-Term Carbon Dioxide Fluxes from a Very Tall Tower in a Northern Forest: Flux Measurement Methodology

BRADFORD W. BERGER,* KENNETH J. DAVIS,+ AND CHUIXIANG YI+

Department of Soil, Water and Climate, University of Minnesota, St. Paul, Minnesota

PETER S. BAKWIN

Climate Monitoring and Diagnostics Laboratory, National Oceanic and Atmospheric Administration, Boulder, Colorado

CONG LONG ZHAO

Cooperative Institute for Research in Environmental Science, University of Colorado, Boulder, Colorado

(Manuscript received 6 January 2000, in final form 28 June 2000)

ABSTRACT

Methodology for determining fluxes of CO_2 and H_2O vapor with the eddy-covariance method using data from instruments on a 447-m tower in the forest of northern Wisconsin is addressed. The primary goal of this study is the validation of the methods used to determine the net ecosystem exchange of CO_2. Two-day least squares fits coupled with 30-day running averages limit calibration error of infrared gas analyzers for CO_2 and H_2O signals to ≈2%–3%. Sonic anemometers are aligned with local streamlines by fitting a sine function to tilt and wind direction averages, and fitting a third-order polynomial to the residual. Lag times are determined by selecting the peak in lagged covariance with an error of ≈1.5%–2% for CO_2 and ≈1% for H_2O vapor. Theory and a spectral fit method allow determination of the underestimation in CO_2 flux (<5% daytime, <12% nighttime) and H_2O vapor flux (<21%), which is due to spectral degradation induced by long air-sampling tubes. Scale analysis finds 0.5-h flux averaging periods are sufficient to measure all flux scales at 30-m height, but 1 h is necessary at higher levels, and random errors in the flux measurements due to limited sampling of atmospheric turbulence are fairly large (≈15%–20% for CO_2 and ≈20%–40% for H_2O vapor at lower levels for a 1-h period).

1. Introduction

Determination of the amount and distribution of carbon sequestration or release by terrestrial ecosystems is essential to understanding the global carbon budget. Global CO_2 mixing ratios measured at sites that are minimally affected by local sources and sinks are lower than that expected for atmospheric accumulation of the total anthropogenic CO_2 emissions, implying the existence of a large carbon sink (Conway et al. 1994). Models, isotopic tracer studies, and measurements of atmospheric O_2/N_2 suggest that a very large portion of this sink is land based and located in the Northern Hemisphere (e.g., Tans et al. 1990; Denning et al. 1995; Ciais et al. 1995a, b; Francey et al. 1995; Keeling et al. 1996). To assess the role that the forests of the north-central United States and south-central Canada play in this scenario, a 447-m television tower located in northern Wisconsin (45.95°N, 90.27°W, 472 m above sea level) has been instrumented to measure mean CO_2 mixing ratio profiles; and fluxes of CO_2, latent heat, and sensible heat using the eddy-covariance method. These measurements provide the opportunity to study the seasonal and diurnal processes of the forest in this region. Uses of the tower measurements include determining accurate values of net ecosystem exchange (NEE) of CO_2 for a large footprint of the forest, calculation of boundary layer CO_2 mixing ratios, estimation of CO_2 entrainment at the top of the boundary layer, validation and constraint of carbon cycle models, testing boundary-layer flux gradient relationships, and extrapolation of upper tropospheric CO_2 mixing ratios.

Measurement of CO_2 fluxes using the eddy-covariance method from towers is not a new concept and has been described in some detail (e.g., Baldocchi et al.

* Current affiliation: Department of Mathematics and Statistics, University of Edinburgh, Edinburgh, Scotland.

+ Current affiliation: Department of Meteorology, The Pennsylvania State University, University Park, Pennsylvania.

Corresponding author address: Bradford W. Berger, Department of Meteorology, The Pennsylvania State University, 512 Walker Building, University Park, PA 16802-5013.
E-mail: bberger@gis.umn.edu

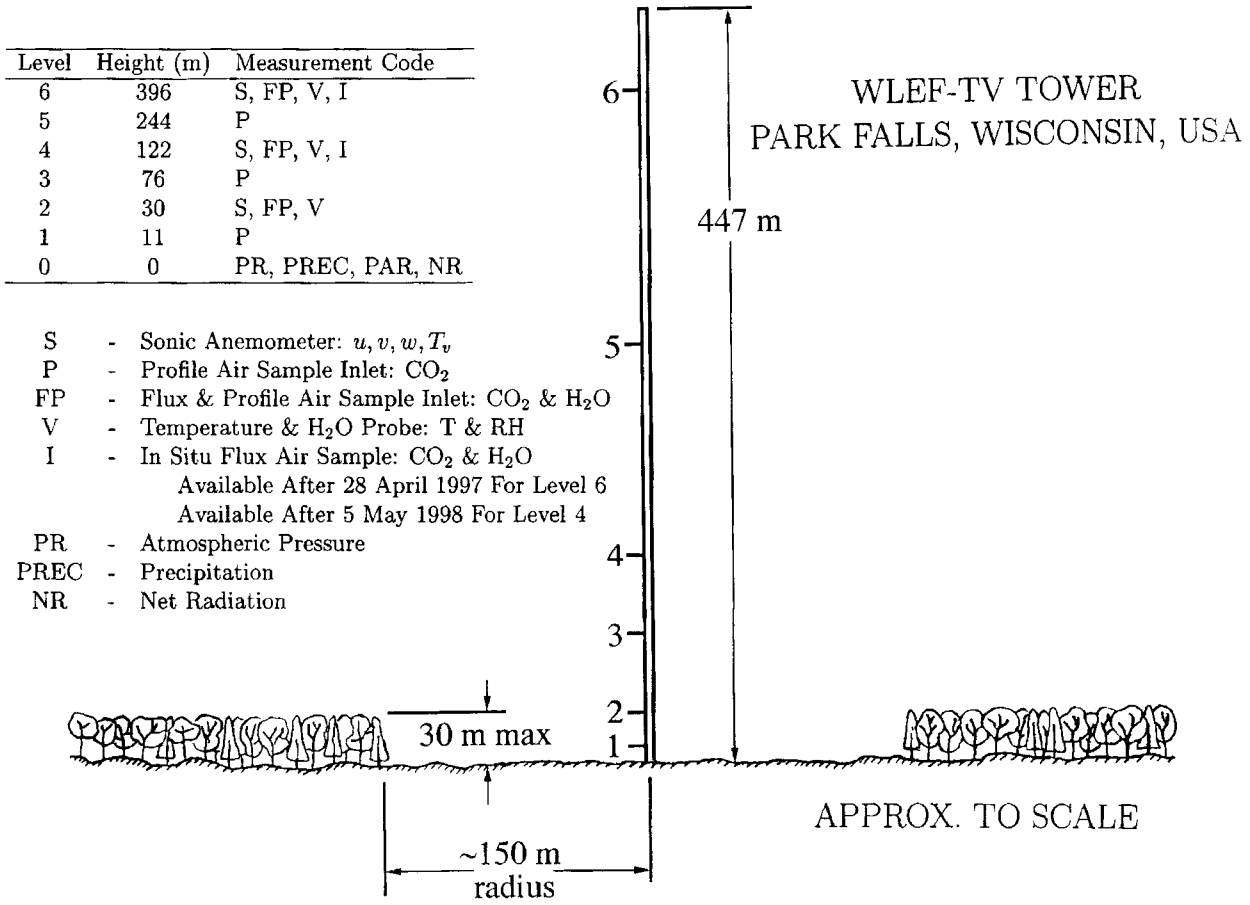

FIG. 1. Schematic of instrument configuration. WLEF-TV tower is located in the Chequamegon National Forest, about 15 km east of Park Falls, Wisconsin. High-rate flux measurements are made at 30, 122, and 396 m. Slow-rate profile measurements are made at 11, 30, 76, 122, 244, and 396 m. Instrument housing at base of tower not shown.

1987; Wofsy et al. 1993; Grace et al. 1995; Goulden et al. 1996a, b; Grelle and Lindroth 1996). Our tower site is one of more than 30 such sites that are part of AmeriFlux[1]; a coordinated effort across the Americas to gain understanding of the biophysical processes that control terrestrial carbon sequestration. The Wisconsin tower is unique among current AmeriFlux sites in its great height and multiple levels of flux instrumentation. Preliminary results from the tower were given by Davis et al. (1996) and the data were used by Yi et al. (2000) to examine the role of advection in our measurements of NEE. This paper establishes the eddy-covariance methodology that will be the basis for future publications.

2. Description of instrumentation

The television tower (WLEF-TV) is located in the Park Falls Ranger District of the Chequamegon National Forest, about 15 km east of Park Falls, Wisconsin. The tower instrumentation configuration is shown schematically in Fig. 1. The system can be divided into two parts: a ''flux'' system where data are stored at 5 Hz and are suitable for obtaining fluxes using the eddy-covariance method; and a ''profiler'' system where data are stored at a slower rate and can be used to determine mean mixing ratio profiles of CO_2 for calculation of the CO_2 rate of change of storage term in the NEE budget, and for calibrating the CO_2 signal from the flux system. Flux data are collected at 30, 122, and 396 m above the ground; and profile data are collected at 11, 30, 76, 122, 244, and 396 m.

The flux instrumentation for each level consists of a sonic anemometer (Applied Technologies Inc., Boulder, Colorado, model SAT-11/3K; or Campbell Scientific, Inc., Logan, Utah, model CSAT3, depending on date) to measure wind and sonic virtual temperature, and an infrared gas analyzer (IRGA) (Li-Cor, Incorporated, Lincoln, Nebraska, model LI-6262) to measure CO_2 and H_2O vapor mixing ratios. Additional instrumentation at the flux levels includes a platinum resistance temperature probe packaged together with a capacitive sensor

[1] More information regarding AmeriFlux can be viewed online at http://cdiac.esd.ornl.gov/programs/ameriflux

TABLE 1. Typical flux IRGA system physical dimensions and operating characteristics. Tube lengths and flow values are approximate. Listed lag times are for tube travel time only and do not include the dis-synchronization time discussed in section 3c.

Level (m)	IRGA position	Tube length (m)	Lag time (s)	Tube inner diameter (m)	Flow rate (L min^{-1})	Reynolds number
396	Trailer	406	87	0.009	17.8	2640
122	Trailer	132	23	0.009	21.9	3250
30	Trailer	40	16	0.009	9.5	1420
396	Tower	5	1.7	0.0032	1.4	592
122	Tower	5	1.1	0.0032	2.2	915

for relative humidity (Vaisala model HMP45C). Data from the temperature/humidity probes are used for calibration of the IRGA which will be discussed in section 3a. The anemometers and temperature/humidity probes are attached to booms projecting ≈3 m from the south-facing side of the tower, and the IRGAs are located in a temperature-controlled room of a mobile truck trailer at the base of the tower. Air sampled within 1 m of each sonic anemometer is continuously supplied to the ''trailer'' IRGAs via a 0.009-m inner diameter tube (DuPont Dekabon type 1300) at approximately 10–22 L min^{-1}, and the pressure at the trailer IRGA sample cell is approximately 390 hPa. The average surface pressure at the site is 958 hPa.

Additional IRGAs were installed in weather-proof enclosures at the 396- and 122-m levels on the tower in late April 1997 and in early May 1998, respectively. These ''tower'' IRGAs provide a backup to the trailer IRGAs and aid in evaluation of the spectral degradation of the CO_2 and H_2O signals due to mixing in the long sample tubes. There is approximately 4 m of 0.0032-m inner diameter Teflon tubing from the air inlet to the tower IRGA sample cell. The pressure in the sample cell is approximately 870 hPa.

Physical dimensions and the typical operating characteristics for the flux IRGA system are listed in Table 1.

A detailed description of the profiler system, its calibration using multiple reference gases, and the data acquisition system for logging both flux and profiler data are described by Zhao et al. (1997). Presentation of the profiler data is given by Bakwin et al. (1998).

3. Data processing

a. Flux IRGA calibration

The flux IRGA output voltages corresponding to CO_2 and H_2O vapor are calibrated using data from the profiler system and the temperature/humidity probes. The calibration method results in flux signals of CO_2 and H_2O in terms of mixing ratios. Fluxes calculated with mixing ratios do not require correction by the heat flux (and H_2O vapor flux for the CO_2 case) (Webb et al. 1980).

The first step in the flux IRGA calibration is to perform a linear fit of the function that represents the CO_2 or H_2O vapor mixing ratio in terms of the IRGA parameters (voltage, pressure, temperature, and in the case of CO_2, the H_2O vapor mixing ratio—all known at 5 Hz) versus the CO_2 or H_2O mixing ratios from the profiler system or the temperature/humidity probes, respectively, for every 2 days of data.

A second step is to perform a weighted running average of the slopes and intercepts over a period longer than 2 days (we are currently using 30 days). The weights are based on the statistical properties of the 2-day fits, with better fits receiving higher weight. Daily slope and intercept values determined by the weighted running average are used to convert the 5-Hz IRGA voltages for that day into mixing ratios for CO_2 and H_2O vapor. These high-rate time series are used to calculate the fluxes.

The IRGA contains an infrared source and detector that are used to monitor the absorptance of infrared radiation by a known reference gas and the gas to be sampled as they are pumped continuously through a reference cell and sample cell, respectively. The IRGA output voltage is proportional to the difference between the detector signals from each cell (Li-Cor 1996). The detector signal is proportional to the photon flux transmitted through the cell and thus is proportional to the density of the gas in the cell. Therefore, the voltage can be expressed as

$$V \propto \rho_r - \rho_s, \tag{1}$$

where ρ is the gas density and the subscripts r and s refer to the reference and sample cell, respectively.

If the dry air CO_2 mixing ratio is defined as $r_c \equiv \rho_c/\rho_d$, where ρ_c is the CO_2 density and ρ_d is the dry air density, the voltage V_c can be rewritten as

$$V_c \propto r_{cr}\rho_{dr} - r_{cs}\rho_{ds}. \tag{2}$$

Our goal is to find r_{cs} in terms of the quantities we know, such as the voltage and cell temperature and pressure. Note that $\rho_{dr} \neq \rho_{ds}$.

Since the partial density of CO_2 is negligible compared to that of dry air and H_2O vapor, we can use the ideal gas law to obtain

$$\rho_d = \frac{pM_d}{T_v R} - \frac{eM_w}{TR}, \tag{3}$$

where p is the total pressure; M_d and M_w are the molecular weights of dry air and water, respectively; T_v is the virtual temperature, R is the universal gas constant; e is the H_2O vapor pressure; and T is the air temperature.

By connecting the reference and sample cell output tubes immediately after the cells, and because the input tubes are in the same temperature environment, we assume that $p_r = p_s = p$ and $T_r = T_s = T$, respectively. These conditions are estimated to hold within less than 1 hPa for the pressure and 0.5°C for temperature, resulting in less than 0.6% combined error in the flux of CO_2 when the system is running in ''differential'' mode

(i.e., $r_{cr} \neq 0$). The system was converted to ''absolute'' mode ($r_{cr} = 0$) in mid-1998, which eliminates the issue of unequal pressure and temperature between the reference and sample cell. Also, $e_r = 0$ because the reference gas is dry. Thus, if we use standard relationships for H_2O vapor pressure and virtual temperature, we can rewrite (2) as

$$V_c \propto \frac{M_d}{R}\frac{T_0}{p_0}\frac{p}{T}\left[r_{cr} - r_{cs}\left(\frac{\varepsilon}{\varepsilon + r_{qs}}\right)\right]. \quad (4)$$

The quantity r_{qs} is the H_2O vapor mixing ratio in the sample cell (obtained below) and $\varepsilon = M_w/M_d = 0.622$. The quantities T_0 and p_0 are arbitrary reference values for temperature and pressure, respectively, that have been introduced to normalize the temperature and pressure. We have chosen $T_0 = 273.15$ K and $p_0 = 1000$ hPa.

We assume that (4) has a linear functional form over a narrow range of CO_2 so that

$$\hat{m}_c\left\{\left[r_{cs}\left(\frac{\varepsilon}{\varepsilon + r_{qs}}\right) - r_{cr}\right]\frac{T_0}{T}\right\} + \hat{b}_c = \frac{p_0}{p}V_c, \quad (5)$$

where R and M_d are absorbed into the slope $\hat{m}_c$. We determine the values of the coefficients $\hat{m}_c$ and $\hat{b}_c$ by performing a linear regression with the unknown sample cell CO_2 mixing ratio, r_{cs}, replaced by the value measured simultaneously by the profiler system.

Finally, we rearrange (5) to yield the mixing ratio for CO_2 as

$$r_{cs} = \left[\left(m_c\frac{p_0}{p}V_c + b_c\right)\frac{T}{T_0} + r_{cr}\right]\left(1 + \frac{r_{qs}}{\varepsilon}\right), \quad (6)$$

with the slope $m_c = 1/\hat{m}_c$ and intercept $b_c = -\hat{b}_c/\hat{m}_c$. The statistics from the regressions used to find the hatted coefficients provide a straightforward way to determine weights for an averaging procedure that smooths variation in the coefficients over periods longer than that over which the fit is performed.

Similarly, the H_2O vapor mixing ratio calculated from the relative humidity and temperature obtained from the temperature/humidity probes and atmospheric pressure measured at the base with an analog barometer (Atmospheric Instrumentation Research, Inc., model AB-2A) and extrapolated to the tower level using the altimeter equation (2.35) of Wallace and Hobbs (1977) should match the H_2O vapor mixing ratio from the flux IRGA. Since the reference cell gas contains no H_2O vapor, the calibration equation for H_2O vapor mixing ratio can be written as

$$r_{qs} = \frac{\left[\left(m_q\frac{p_0}{p}V_q + b_q\right)\frac{T}{T_0}\right]}{1 - \frac{1}{\varepsilon}\left(m_q\frac{p_0}{p}V_q + b_q\right)\frac{T}{T_0}}. \quad (7)$$

It may be noted that, excluding the water vapor correction, (4) has the same form as presented in the IRGA operation manual [Li-Cor 1996, Eq. (3–4)]. Because the IRGA response is nearly linear in the range encountered over the 2-day fit period, we find it only necessary to calibrate using a linear function instead of the higher-order calibration polynomial function suggested by the manufacturer. A 2-day interval has been found to be long enough to capture sufficient variation in the mixing ratios to determine a fit, and short enough to allow the instrument to be locally calibrated within a linear range and to track instrument drift. Seasonal variability of the range (and thus the fit slope) is most prominent for H_2O vapor.

The slopes m_c and m_q in (6) and (7) are nearly proportional to the variances of r_{cs} and r_{qs}, respectively. This is because most of the variance is contained in the voltage while the IRGA pressure and temperature are fairly stable. Thus, to accurately calculate fluxes of CO_2 and H_2O vapor, it is more important to accurately determine the slope than the intercept of the fits.

The precision of the CO_2 measurement from the profiler that is used to calibrate the fast IRGA should be better than 0.1 ppm (Bakwin et al. 1998). The precision of the humidity probe has been estimated to be approximately $\pm 0.15\%$ RH (Ivan Bogoev 2000, personal communication), or in terms of the tower environment ± 0.08 g kg^{-1} in the worst case. Since these errors should be random and the calibration is performed with 2-min averages over 2 days, the slope error due to the precision has been estimated to be less than 0.1% for H_2O, and even smaller for CO_2. The 2-min averaging time for each data point should also minimize error due to hysteresis of the humidity probe.

The motivation for the calibration method described derives from the availability of the high precision CO_2 and H_2O vapor values used for determining the slopes. The cost and complexity of running calibration gases through the fast IRGAs were felt to be unneccesary since the CO_2 profile system was already in place and the temperature/humidity probes are relatively inexpensive.

Figures 2a,b show typical 2-day fits (15–16 May 1998) of data used for finding the slopes and intercepts. During the growing season, when fluctuations in CO_2 and H_2O vapor are large, the correlation coefficients (r^2) for the fits are usually near unity. The r^2 values drop somewhat during the winter months when the fluctuations are smaller. Figures 2c,d show the slopes from the 2-day fits superimposed on the 30-day weighted running average for CO_2 and H_2O, respectively. The seasonal change in the H_2O calibration coefficients due to the IRGA response can be clearly seen.

The uncertainty in calculated CO_2 and H_2O fluxes due to random error in the calibration is estimated to be approximately 2%–3%. This is a standard error based on the distribution of the 2-day fits about the weighted running average and assuming that this distribution is

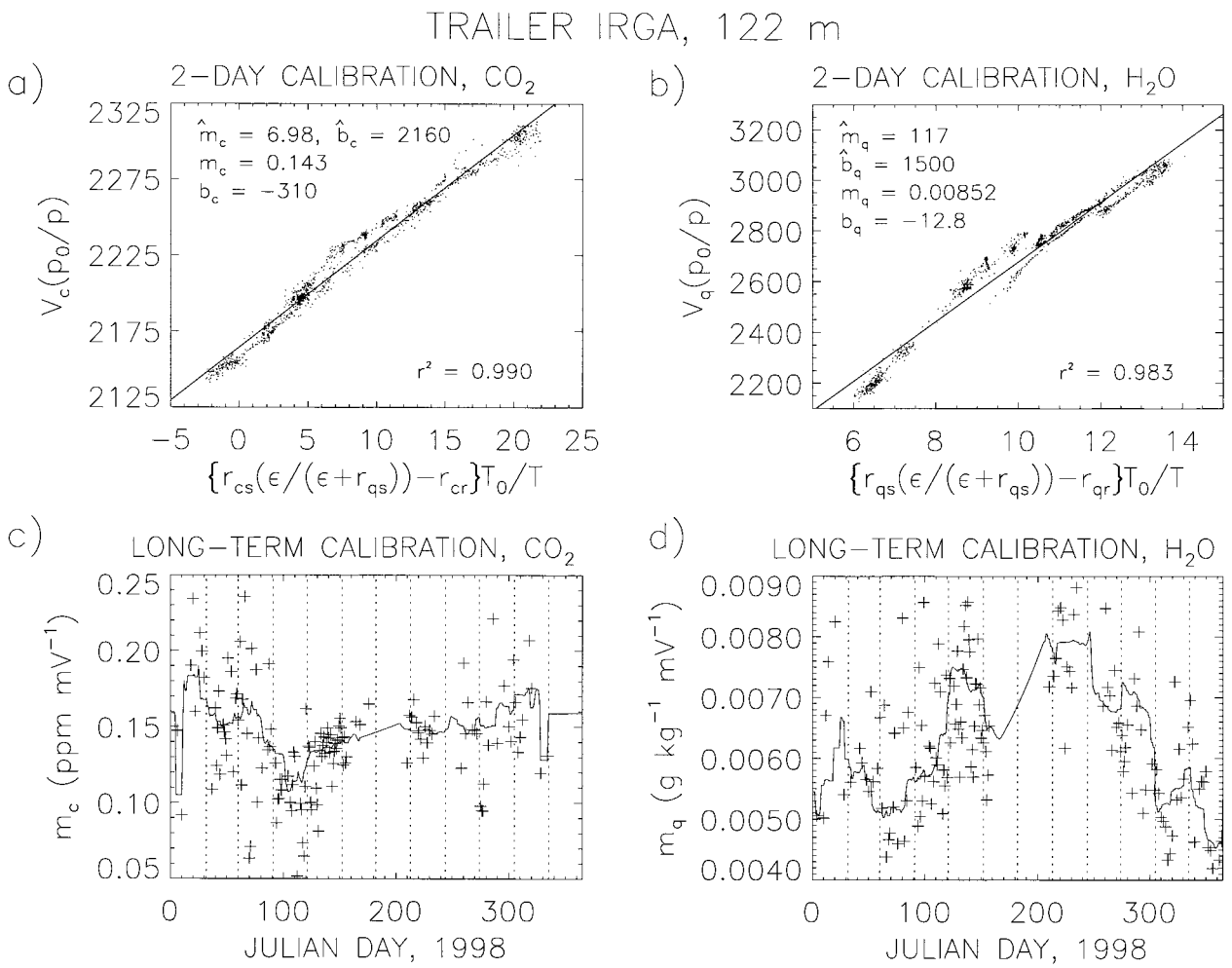

FIG. 2. Trailer IRGA calibration, 122-m tower level. Typical 2-day fits of 2-min averaged data (from 15–16 May 1998) used to determine slope and intercept values for (a) CO_2 and (b) H_2O vapor. Long-term calibration slope from 1998 data for (c) CO_2 and (d) H_2O vapor where "+" is from 2-day fits and solid line is the 30-day weighted running average used to calibrate signals for flux calculations.

steady over the year. Slightly less scatter is observed in the fits during the growing season, therefore the uncertainty should be less during the portion of the year when fluxes are largest. The uncertainty may be larger during the winter months, but fluxes are small at this time. The uncertainty will increase if the number of usable 2-day fits in the running average window decreases.

b. Sonic anemometer rotation correction

Wind velocities from the sonic anemometers are rotated into a coordinate system aligned with the local mean streamlines. McMillen (1988) and Baldocchi et al. (1988) discuss these rotations in detail.

The rotation is defined by two angles. Using 1-h of data, the mean wind direction ϕ is found with the horizontal wind components u and v, then a tilt angle θ is found by rotating about the mean cross-wind direction to where the average vertical velocity w becomes zero. A misaligned sonic anemometer in a uniform flow would exhibit a perfect sinusoid to describe tilt angle versus wind direction. Therefore, a sine function is first fitted to the hourly wind direction and tilt angle data. To account for curvature in the streamlines due to local topography and the tower, the sine function is then subtracted from the data and a third-order polynomial function is fitted to the residual. The sine function and polynomial are added to obtain the complete rotation fit, which is then used to align each hour of sonic anemometer data with the local mean streamlines. This procedure results in a finite average vertical wind velocity, $\overline{w}$. Preliminary analysis shows that although hourly values may not have enough accuracy ($\sigma_{\overline{w}} = 0.1$ m s^{-1}) for determining synoptic-scale lifting or subsidence at that hour, averages over 1–2 days should be suitably accurate ($\sigma_{\overline{w}} = 0.01$ m s^{-1}) to detect synoptic motions and may provide insight into vertical advection issues in the computation of NEE of CO_2 (Yi et al. 2000).

Figure 3 shows an example of the resulting fits for several months of data. When the wind blows from the

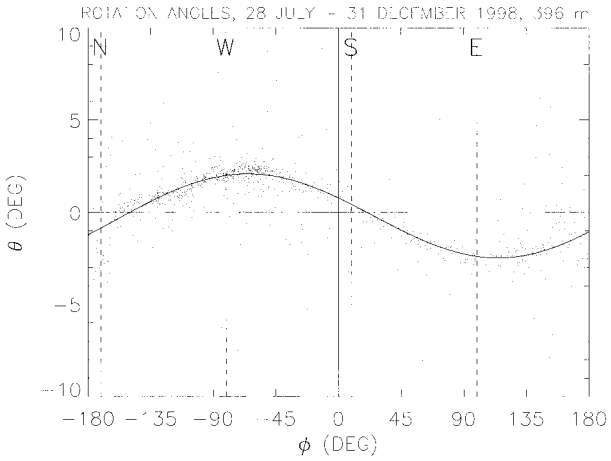

FIG. 3. Sonic anemometer rotation correction for 28 Jul–31 Dec 1998 (1897 usable hours), 396-m level. Tilt angle θ vs wind direction ϕ. Fit is $\theta = 3.82 \times 10^{-2} \times \sin(\phi + 2.68) + 2.23 \times 10^{-4}\,\phi^3 + 5.58 \times 10^{-5}\,\phi^2 - 1.75 \times 10^{-3}\,\phi - 3.42 \times 10^{-3}$ rad. Wind from the north is blocked by the tower.

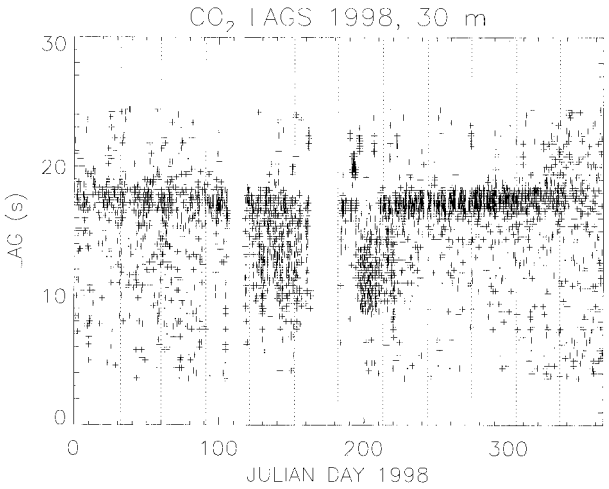

FIG. 4. Hourly CO_2 lag times (s) for trailer IRGA from 30-m level for 1998. Points are from periods where a discernable peak was found in the lagged covariance within a window of lag times expected for that level. Lag times include the dis-synchronization time (approximately 10-s maximum) described in section 3c.

north, the tower impedes the flow. This is the most likely reason for the larger variance of hourly θ values for wind in this direction; however, the influence of the tower is not observed at the 30- and 122-m levels. The distortion at 396 m may be due to a broadcast antenna mounted to the tower near the instrumentation only at that level.

c. Lag times

Calculating eddy covariance fluxes requires simultaneous measurements of wind and scalar quantities. The long tubes from the air sample inlets to the IRGAs at the base of the tower induce substantial delay in the signals used for calculating the CO_2 and H_2O fluxes. This delay can be determined by lagging the rotated wind signal until maximum covariance is obtained (Fan et al. 1990). However, this delay may change slightly due to changing flow rates in the tubes from factors such as pumping variation or density and viscosity changes. Lag times may also change in our case, due to poor synchronization of the remote computer that acquires the sonic anemometer data and the main data acquisition computer that acquires the trailer IRGA data and stores all of the data. However, this synchronization error only results in a fixed lag time between the start time of a particular hour-long data file for the sonic and the start time of an hour file of IRGA data. The dis-synchronization can vary from hour to hour up to approximately 10-s maximum. Although the synchronization-induced lag variation is not ideal, it is not considered to be a serious problem since the lag time can be determined. The computer synchronization has recently been improved.

The separation distance from the air sample inlet to the sonic anemometer is approximately 1 m. Lag times resulting from this displacement should be $<$0–2 s depending on wind speed and direction, but this lag will be included in the lag time determined with the maximum covariance method. Because the turbulence scales contributing to the covariance are much larger than 1 m (see section 3e), the separation will have a minimal effect on the estimation of fluxes.

Figure 4 shows a typical example of the variation in the lag time between the vertical velocity signal and the CO_2 signal from the trailer IRGA for the 30-m level. The lag times include the computer dis-synchronization time. All points in Fig. 4 are from periods where the lagged covariances were considered to be unambiguous, that is, a discernable peak was found within a window of lag times expected for that level. It is important to keep track of these lags on an hourly basis to ensure correctly calculated fluxes; one fixed lag time is insufficient. If a flux is not large enough to allow detection of the lag time, as sometimes occurs at night due to low turbulence levels, adjacent hours are used to estimate the lag.

When the lagged covariance shows a clearly detectable peak, a lag time can be determined within approximately ± 1 s for CO_2 and ± 3 s for H_2O. These times correspond to variation in the calculated flux of 1.5%–2% and 1% for CO_2 and H_2O, respectively. The variation in CO_2 flux is proportionally larger because the CO_2 lagged covariance typically has a sharper peak than H_2O.

d. CO_2 and H_2O signal spectral corrections

Spectral degradation of the CO_2 and H_2O flux signals is expected due to the long tubes that carry sample air to the trailer IRGAs. This problem can be attributed

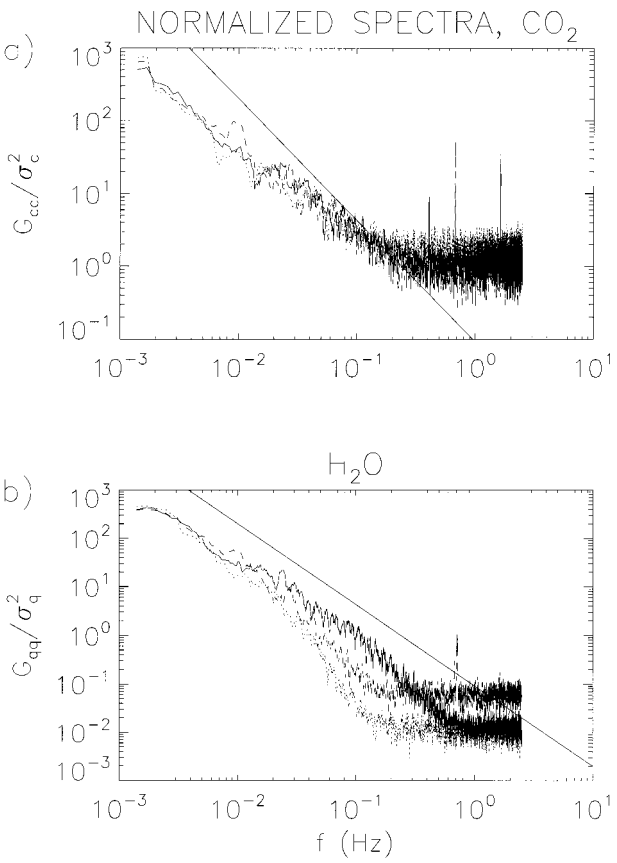

FIG. 5. Spectra normalized by the partial variance (see description in text) for (a) CO_2 and (b) H_2O vapor from trailer IRGA for the 30- (solid), 122- (dashed), and 396-m (dotted) level. The CO_2 spectra show little relative degradation at least up to where noise becomes apparent at approximately 0.2 Hz. The H_2O vapor spectra show relative degradation that increases with height. Solid line of $-5/3$ slope shown for comparison.

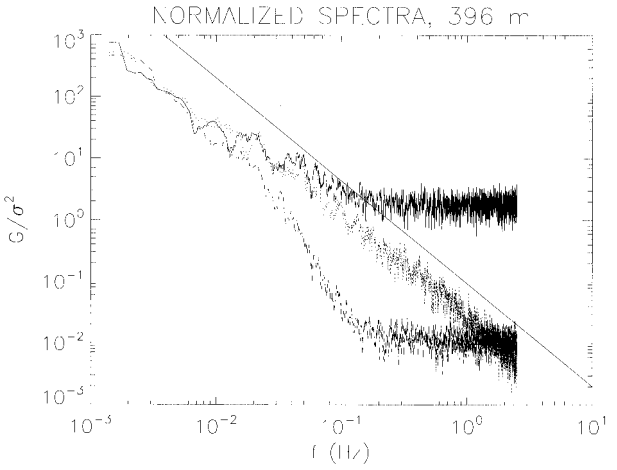

FIG. 6. Spectra normalized by the partial variance (see description in text) for temperature (dotted), CO_2 (solid), and H_2O vapor (dashed) from trailer IRGA for the 396-m level. The CO_2 and temperature spectra match shape at least up to where noise becomes apparent in the CO_2 spectrum. H_2O vapor shows significant degradation that increases with increasing frequency. All spectra are well matched for frequencies below 0.02 Hz. Solid line of $-5/3$ slope shown for comparison.

primarily to nonuniform velocity across the cross section of the tube as well as interaction with the tubing walls. These diffusive mechanisms will attenuate high frequencies (smaller scales) more than low frequencies (larger scales) and result in underestimation of CO_2 and H_2O fluxes.

Figures 5a,b show typical spectra for CO_2 and H_2O from the trailer IRGAs for all levels. In order to match the levels of the spectra at low frequency, each spectrum is normalized by dividing every value in the spectrum by the variance contributed by the lowest frequencies. We chose $f \approx 6 \times 10^{-3}$ Hz as the upper limit for computing this ''partial'' variance. The CO_2 spectra in Fig. 5a show no relative degradation, at least up to frequencies greater than 0.2 Hz where the signal becomes dominated by instrumental noise. The H_2O spectra in Fig. 5b, however, clearly show increasing attenuation with increasing tower height (i.e., tubing length). Comparison of the low-frequency portion of CO_2 and H_2O nonnormalized spectra from the trailer IRGAs with that from the tower IRGAs found no difference in spectral power (not shown) confirming that there is little low-frequency degradation.

Spectra of temperature, H_2O vapor, and CO_2 from a given location should be similar in shape (Ohtaki 1985) if they are perfectly measured. Virtual temperature obtained from the sonic anemometers should give the best representation of the true atmospheric spectra for all scalars since it is from a fast-response, open-path instrument. Humidity and cross-wind corrections to the temperature signal are described by Hignett (1992) and we currently employ the humidity correction. The crosswind correction has been estimated to affect the measured sensible heat flux by no more than 1% when the flux is larger than 5–10 W m^2 and spectral degradation of the temperature due to crosswinds is minimal. The crosswind correction will be implemented in the near future. Spectral degradation due to line averaging error [the effect of measuring the temperature over the distance between the sonic transducers and discussed by Moore (1986)] has been estimted to be less than 2% at 0.3 Hz (the typical highest frequency of scales contributing to the fluxes at the lowest level, see section 3e), and far less at lower frequencies.

Figure 6 compares the CO_2 and H_2O spectra to the temperature spectrum at the 396-m level and is representative of the other levels. Similarity of the CO_2 and temperature spectra confirms that CO_2 is not seriously degraded, at least up to the frequency of the instrumental noise.

Early work studying diffusion in tubes with laminar and turbulent flows was done by Taylor (1953, 1954). His work was used by Lenschow and Raupach (1991) to analytically estimate spectral degradation due to sam-

pling tubes in order to determine the transfer function $\phi(f)$ that gives the attenuation at each frequency f such that

$$G\phi^2(f) = G_d, \tag{8}$$

where G is the perfectly measured spectrum of some scalar quantity and G_d is the degraded spectrum. Using Taylor's representation of the diffusion in the tube for turbulent flow, ϕ is found to be

$$\phi(f) = \exp(-Kf^2), \tag{9}$$

with

$$K = \frac{79.7aL}{\mathrm{Re}^{1/8}U^2}, \tag{10}$$

for laminar flow in the tube, and

$$K = \frac{0.41\mathrm{ReSc}aL}{U^2}, \tag{11}$$

for turbulent flow. Here K is a function of the tubing radius a; tubing length L; mean flow velocity U; the Reynolds number $\mathrm{Re} = 2aU/\nu$, where ν is the molecular viscosity; and in the case of turbulent flow, the Schmidt number $\mathrm{Sc} = \nu/\nu_D$, where ν_D is the coefficient of molecular diffusion.

Massman (1991) presents a numerical analysis of spectral attenuation including tabulated values that may be used to calculate the value of K in (9). He describes an attenuation coefficient based on Reynolds number that differs for particular scalars to take into account differing Schmidt number.

Goulden et al. (1996b) discuss an alternative method for correction of the CO_2 fluxes. Assuming that the temperature signal is nearly perfect, they empirically determine the time constant for a low-pass filter that allows them to mathematically degrade the temperature signal to mimic the degradation of the CO_2 signal by the IRGA and tubes as a system. Then the ratio of the nondegraded to degraded heat flux should match the ratio of the corrected to uncorrected CO_2 flux such that

$$\overline{w'c'}_{\text{corrected}} = \overline{w'c'}_{\text{uncorrected}} \frac{\overline{w'T'}}{\overline{w'T'_d}}, \tag{12}$$

where w', c', T', and T'_d are the fluctuating components of the vertical velocity, the CO_2 mixing ratio, the temperature and degraded temperature, respectively, and the overbar denotes time averaging. This presents a simple and effective way to repair CO_2 *and* H_2O fluxes if the appropriate filter can be found.

Goulden et al. model the degradation process as a recursive low-pass digital filter described by McMillen (1988) and Moore (1986) as

$$T_{d_i} = \alpha T_{d_{i-1}} + (1 - \alpha)T_i, \tag{13}$$

where T_{d_i} is the degraded temperature T_d at time t_i, $T_{d_{i-1}}$ denotes a value at the previous time step t_{i-1}, T_i is the nondegraded temperature at time t_i, and $\alpha = \exp[-\delta/\tau]$ where $\delta = t_i - t_{i-1}$ (the time step between points), and τ is an empirically determined time constant (J. W. Munger 1998, personal communication). Goulden et al. find τ based on an exponential fit to the relaxation of the CO_2 signal after an addition of CO_2 calibration gas at the inlet is shut off. If the selected τ is correct, the spectrum of the degraded temperature will have the same shape as the spectrum of the uncorrected CO_2 or H_2O signal. At our site, it is not practical to determine τ using the method above, and therefore it can only be found iteratively by choosing a τ and seeing if the resulting degraded temperature spectrum matches the spectrum of the uncorrected CO_2 or H_2O signal. This is very inefficient computationally and so a more direct method of finding the degraded temperature signal was desired.

One possible method is to degrade the temperature spectrum using a transfer function ϕ calculated from the Taylor-based theory of Lenschow and Raupach or from the numerical results of Massman. Then the degraded temperature time series T_d can be found by taking the inverse Fourier transform of the degraded spectrum. The combination of these steps can be written as

$$T_d = \mathrm{Real}(\mathrm{IFT}\{\hat{\phi}[\mathrm{FFT}(T)]\}), \tag{14}$$

where IFT and FFT denote the inverse Fourier transform and the Fourier transform, respectively, and where $\hat{\phi}$ is ϕ and its mirror image so that $\hat{\phi}$ corresponds to the double-sided frequency values obtained from the FFT of T. The real part of the IFT gives T_d.

Based on typical values of flow through the sample tubes, the range of K for all tower levels is estimated to be between 0.7 and 2.7 s^2 based on the Lenschow and Raupach formulation. Using the tabulation of Massman, K is estimated to be between 4.6 and 20.9 s^2 for H_2O and 6.1 and 28.8 s^2 for CO_2. Figure 7 shows T and H_2O spectra for a typical midday hour at the 122-m level. Also shown is the theoretical curve of the degraded temperature generated using $K = 14.2$ s^2, the maximum attenuation for that level based on the tabulation for H_20 of Massman for $\mathrm{Re} = 2300$. For the case shown, the actual $\mathrm{Re} = 2850$ so the curve should overestimate the degradation, but it is clear that even when ϕ is overestimated the theory does not capture the attenuation actually seen in the H_2O spectrum for our instrumentation. However, it is possible to determine a ϕ based directly on the spectra. Fits of the normalized spectra give ϕ^2 as

$$\phi^2(f) = \frac{\left(\dfrac{G_{qq}}{\sigma_q^2}\right)_{\text{FIT}}}{\left(\dfrac{G_{TT}}{\sigma_T^2}\right)_{\text{FIT}}}, \tag{15}$$

where G represents the one-sided spectrum of H_2O vapor (denoted by q) or temperature (T), σ^2 is the partial variance for H_2O or temperature, and the FIT subscript

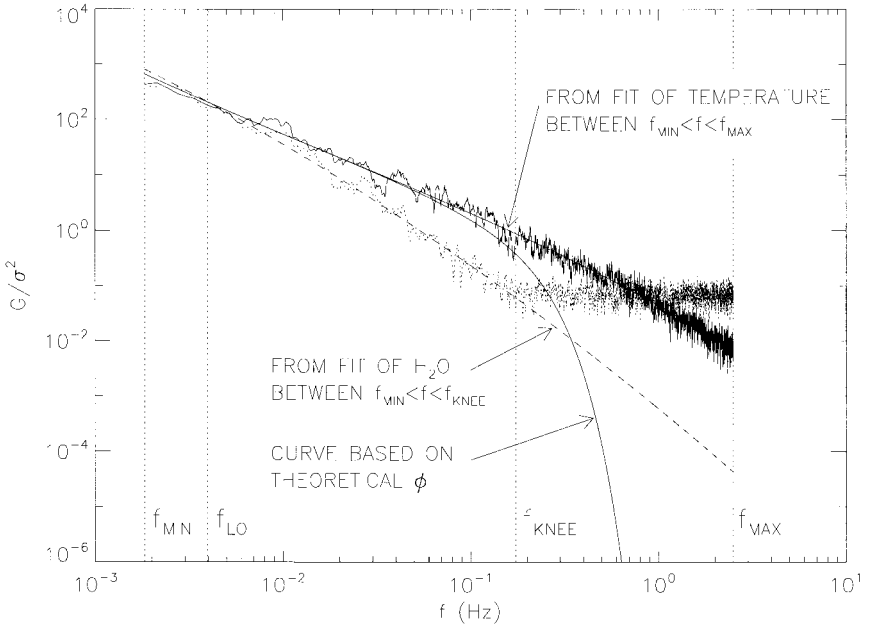

FIG. 7. Typical hourly spectra (temperature: solid; H_2O vapor: dotted) and fits (temperature: solid; H_2O vapor: dashed) at 122-m level used to determine spectral attenuation $\phi^2(f)$ in Eq. (15). Also shown is curve from degraded temperature (smooth solid) generated with Eq. (14) using theoretical ϕ (Eq. 9) determined with maximum attenuation ($K = 14.2$ s^2) for H_2O vapor based on tabulation of Massman (1991) at Re = 2300. The actual Re = 2850, thus the curve should overestimate degradation; however, comparison with the H_2O vapor spectrum shows that it underestimates the degradation observed.

denotes that the quantity is a curve fit to the data by least squares. The coefficients for a second-order polynomial fit of the H_2O spectrum are found by fitting the spectrum from the minimum frequency (f_{min} in Fig. 7) up to the frequency where the noise becomes apparent (f_{knee}). Finding f_{knee} is done using a wavelet edge detector similar to that described by Davis et al. (2000). The fitted H_2O spectrum is then generated across the full frequency band (f_{min} to f_{max} where f_{max} is the Nyquist frequency) and used in (15). The full frequency band is used to find the coefficients for a second-order fit of the temperature. Below the highest frequency where the fits of the spectra are equal (f_{lo}), ϕ is assumed to be unity. Once ϕ is determined, the degraded temperature can be found with (14) and the corrected latent heat flux found with an equation analogous to (12).

Although suitable for correcting the H_2O fluxes, the spectral fit method of finding ϕ outlined above cannot be used for CO_2 because any degradation to the CO_2 signal is hidden in high-frequency noise. Fluxes for CO_2 are currently being corrected by using ϕ calculated with the theory of Lenschow and Raupach (1991) using (9)–(11).

In addition to spectral attenuation, phase shift (dispersion) may occur due to the tubes. The lag time mentioned in section 3c (a fixed time delay) imparts a linear phase shift with frequency, but if the lag is removed by shifting the time series, phase shift from other mechanisms may remain. Shaw et al. (1998) discuss this issue for a system modeled by a time constant τ. For the recursive low-pass digital filter given by (13) the phase relationsip is

$$\omega_\tau(f) = \tan^{-1}\left[-\frac{\alpha \sin(2\pi f\delta)}{1 - \alpha \cos(2\pi f\delta)}\right]. \qquad (16)$$

Although not mentioned explicitly in Goulden et al. (1996b), according to S. C. Wofsy and J. W. Munger (2000, personal communication), they use a subtle variation to (12) where the vertical velocity is degraded similarly to T using (13) (w_d) and it is substituted into the degraded heat flux $\overline{w_d'T_d'}$ and the uncorrected CO_2 flux $\overline{w_d'c'}_{\text{uncorrected}}$. This keeps the signals in phase and maximizes the degraded flux correlations. Although this changes the nondegraded to degraded flux ratios, the corrected CO_2 (or H_2O) flux should be the same as that given by (12) on average.

We have found that the phase between the velocity and scalar quantities is minimally altered by our system. This implies that degrading the temperature signal using the spectral fit method (which does not alter the phase) and then using (12) to determine the correction is appropriate. Figure 8 shows phase spectra from a typical midday hour between temperature and H_2O, $-CO_2$ (which provides a more clear plot since $+CO_2$ is 180° out of phase with temperature at this time period), the temperature degraded using (13) with $\tau = 6$ s (the τ value necessary to make the degraded temperature spec-

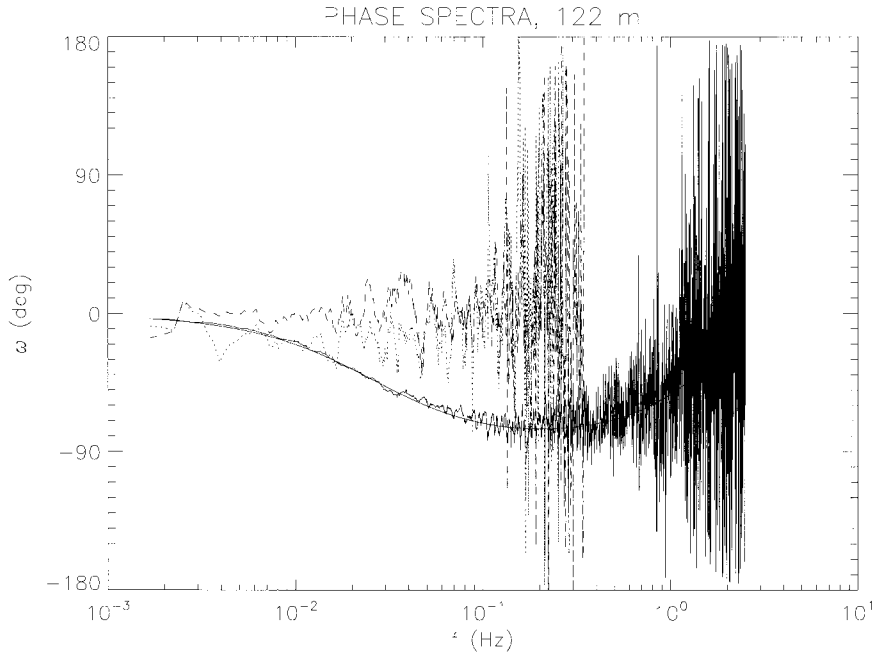

FIG. 8. Phase spectra from a typical mid-day hour for temperature compared with CO_2 (dashed), H_2O vapor (dotted), and degraded temperature T_d from the recursive low-pass digital filter given by Eq. (13) with $\tau = 6$ (solid) for the 122-m level. Theoretical curve of phase given by Eq. (16) for the filter (smooth solid) matches phase between temperature and degraded temperature. Phase spectra for CO_2 and H_2O vapor have been truncated at higher frequency for clarity.

trum match the H_2O spectrum), and the corresponding ω_τ from (16). It is clear that H_2O and CO_2 are not appreciably degraded in phase up to at least 0.1 Hz where the calculated phase passes from $\pm 180°$ to $\mp 180°$ (''wrapping''), and that our system is not modeled well by the filtered signal. For the case shown, the flux contributed by scales corresponding to $f > 0.1$ Hz is approximately 4% of the total. Additionally, the heat flux calculated from the degraded temperature obtained by the spectral fit method (no phase shift) differs from the flux using the filter method [phase shifted by (13)] by only 2%. This indicates that the error due to phase degradation is minimal. Additional justification for neglecting the phase is given by Leuning and Moncrieff (1990) and Leuning and King (1992), who discuss dispersion effects studied by Philip (1963), concluding that the speeds of different scales through a tube are nearly equal if $\Omega < 10$ with $\Omega = 2\pi f a^2/\nu_D$. For our system we have estimated $\Omega \leq 4.0$ for $f < 1$ Hz.

Figures 9a,b show a comparison of spectrally corrected and uncorrected diurnally averaged fluxes for CO_2 and H_2O vapor from both the trailer and tower IRGA signals at the 122-m level. Note that H_2O presents good agreement between the corrected fluxes, with the uncorrected flux from the trailer IRGA signal being the most degraded. For the CO_2 flux, the corrected and uncorrected curves are virtually identical. However, the trailer and tower show some disagreement. Calibration error may account for some of this discrepancy. Table 2 lists the approximate underestimation of CO_2 and H_2O fluxes for the trailer and tower IRGAs from examination of long-term spectral corrections. The ϕ of Lenschow and Raupach strongly attenuates small turbulence scales, thus the night values for CO_2 flux correction are larger due to smaller turbulence scales typically dominating at night. The correction to H_2O, however, is influenced by much larger scales and has been found to have little diurnal sensitivity. The reduction in flux underestimation with increasing height is also due to scales, where scale size increases with height. The trailer IRGAs consistently require more correction than those on the tower, although the underestimation of H_2O flux from the tower IRGAs is not negligible ($\approx$12%).

e. Scale and random error analysis of fluxes

The eddy covariance method requires that the flow be stationary and that all flux-carrying eddies are sampled for an accurate estimation of the flux. Provided that the flow is stationary, an ogive provides a check on the necessary condition of sampling all flux-carrying scales (Desjardins et al. 1989; Friehe et al. 1991). An ogive is defined as the cumulative sum of a cospectrum from high to low frequency and thus has a value equal to the covariance or flux at the lowest frequency. Ogives that have an asymptotic shape toward the highest and lowest frequencies suggest that all flux-carrying scales are contained in the sample period. Figure 10 presents ogives

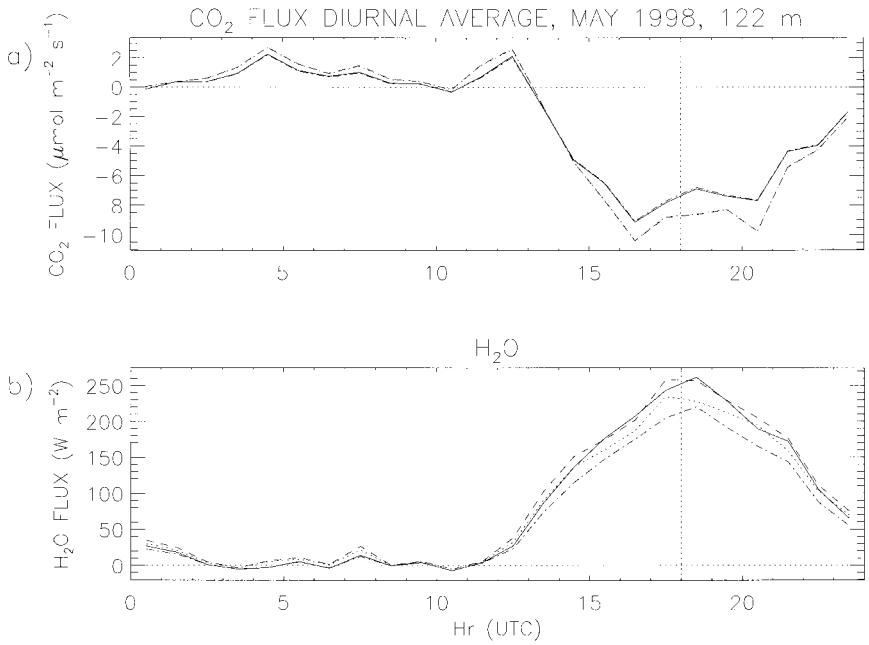

FIG. 9. Comparison of spectrally corrected and uncorrected diurnally averaged fluxes for (a) CO_2 and (b) H_2O vapor from trailer and tower IRGA signals at the 122-m level for May 1998. Trailer corrected (solid), tower corrected (dashed), trailer uncorrected (dash–dot), and tower uncorrected (dotted). Vertical dotted line represents solar noon.

from all tower levels for sensible heat flux based on 2-h sample periods centered at every hour of a day except 0000 and 2400 UTC. Daytime heat fluxes are large and positive, and are the result of the contribution of a wide range of scale sizes. Nighttime heat fluxes are small and negative, and the range of flux-contributing scale sizes is decreased. Flux-carrying scale size also increases with altitude. These observations are consistent with buoyancy dominating the daytime convective regime, shear dominating at night, and scales decreasing in size closer to the surface. Dashed lines denoting 2-, 1-, and 0.5-h sample times show that although 0.5 h may be an acceptable period for flux calculations at the lowest level, at least 1 h is necessary to allow the ogives to converge at the highest level. This supports the choice of 1 h as the period for flux calculations at all tower levels at WLEF. It also adds confidence to fluxes calculated over 0.5 h at the many canopy-level flux towers being used throughout the world. Additionally, Fig. 10 makes it clear that the sample frequency of 5 Hz is adequate for resolving the high-frequency scales contributing to the flux.

TABLE 2. Approximate underestimation (%) of CO_2 and H_2O flux for trailer and tower IRGAs.

Level (m)	IRGA position	CO_2		H_2O
		Day	Night	
396	Trailer	1	7	16
122	Trailer	1.5	9	19
30	Trailer	5	12	21
396	Tower	<0.1	1	13
122	Tower	<0.1	1	11

Based on theory developed by Lenschow and Stankov (1986), the relative error, a, of a flux value can be estimated using the integral length scale of the flux, the cross-correlation coefficient for the flux variables, and the length over which the flux measurement is made. The relative error of flux F is defined as $a \equiv \sigma_F/\langle F \rangle$, where $\langle F \rangle$ is the ensemble average. Figures 11a,b show how a varies with height normalized by the boundary-layer height, z/z_i, for sensible heat flux and CO_2 flux determined over hourly periods during the convective times of 10–11 May 1998. Especially at higher levels in the boundary layer, the relative error can be quite large, on the order of the flux value itself. This result is not unexpected, Lenschow and Stankov show that large averaging times are necessary to reach low relative error levels, with momentum flux requiring the longest averaging length. At the lower levels, relative error for heat flux is less than 20%; however, for CO_2 flux, the relative error can be up to 40%–50%. These relative error values should be similar for measurements over any forest canopy. The only way to reduce the relative error is to increase the length over which the turbulence is averaged; however, care must be taken to avoid averaging times that exceed the time over which the flow is stationary, such as the transition from evening to daytime regimes. It should be noted, however, that even though the relative error may be fairly large for a single flux measurement, the long-term average of the flux will

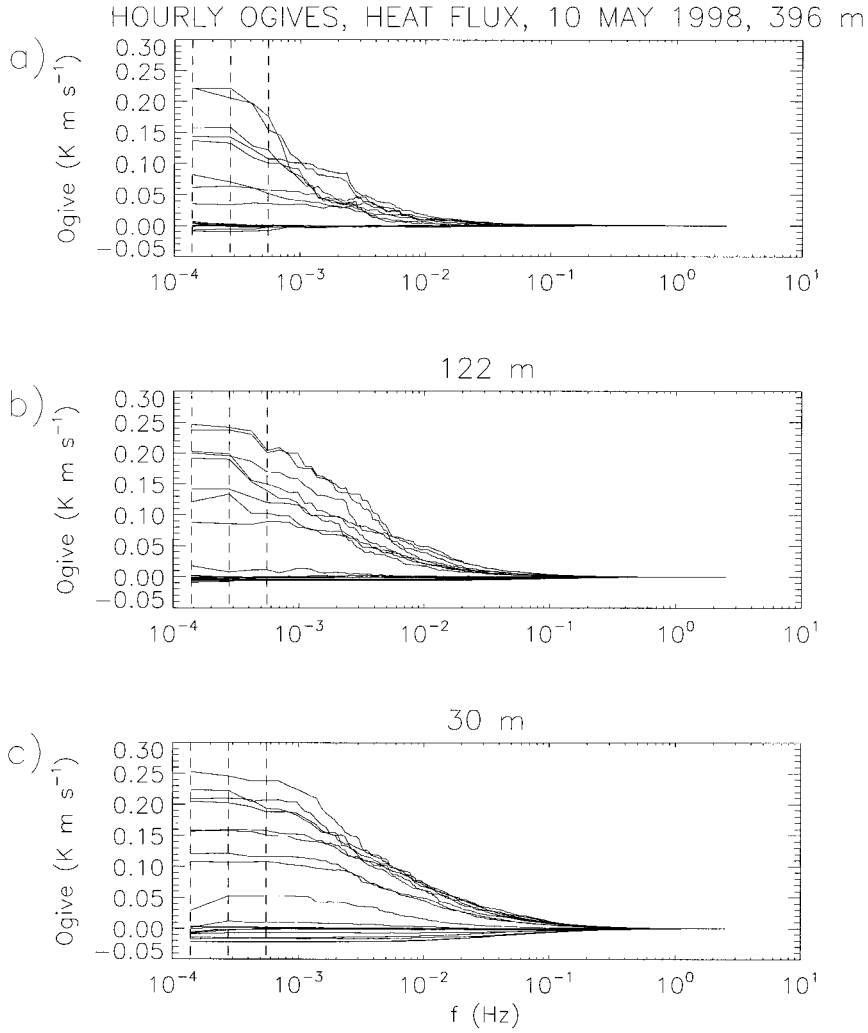

FIG. 10. Hourly ogives based on 2-h periods 11 May 1998 for sensible heat flux at the (a) 396-, (b) 122-, and (c) 30-m levels. Nighttime fluxes are negative due to surface cooling. Flux-carrying scale size increases with altitude and decreases at night, which is consistent with buoyancy dominating the daytime convective regime and shear dominating at night. Dashed vertical lines correspond to time periods of 2, 1, and 0.5 h.

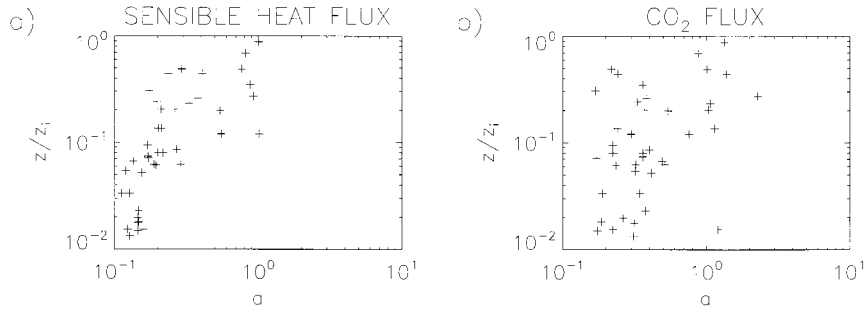

FIG. 11. Relative error *a*, with height normalized by the boundary-layer height, z/z_i, for (a) sensible heat flux and (b) CO_2 flux, based on the theory of Lenschow and Stankov (1986). Errors were calculated from 1-h periods during the convective times of 10–11 May 1998.

have significantly less error because the relative errors are random (Moncrieff et al. 1996). Another important aspect of the relative error with respect to our site, where multiple levels are used, is that the measurements at different levels are not completely independent; the relative error in the difference between the fluxes from two different levels should be less than that implied by the independent relative error of each measurement. The relative error of the difference will depend on the coherence of the turbulence between the levels. This discussion is beyond the scope of this paper.

4. Conclusions

The methodology and instrumentation to measure fluxes at three levels on a very tall tower in northern Wisconsin have been described. The primary steps necessary for processing the data from the tower are calibration of the IRGAs measuring the CO_2 and H_2O vapor mixing ratios, obtaining long-term fits of the angles required to rotate the sonic anemometer data into a defined reference frame, and the determination of lag times and spectral corrections necessitated by the long tubes that carry sample air to the IRGAs. Uncertainty in the flux related to calibration and lag determination were found to be minimal ($<3\%$). Underestimation of the flux due to spectral degradation is small to moderate for CO_2 ($<5\%$ during the day, $<12\%$ at night), and moderate for H_2O ($<21\%$), but these underestimations are correctable. The largest uncertainty in estimating eddy covariance fluxes is from the random nature of turbulence where relative uncertainties of the order of the flux itself may occur when scale sizes are large and the averaging times are short, but is generally $<15\%$–40% for 1-h averaging periods at the lower levels. These uncertainties are inherent in the eddy covariance method itself, but long-term flux averages will have far less error. Assuming that spectral degradation can be corrected and excluding random uncertainty in the flux measurements the total flux measurement uncertainty is estimated to be $\approx 2\%$–4%.

Acknowledgments. This research was funded in part by the National Institute for Global Environmental Change through the U.S. Department of Energy (Cooperative Agreement DEFC03-90ER61010). Any opinions, findings, and conclusions or recommendations expressed herein are those of the authors and do not necessarily reflect the views of DOE. From the University of California, Irvine, we thank Scott Miller for help with the phase analysis, and thanks is given to Perry Fuehrer and Djamal Khelif for helpful discussions related to mathematical details of the spectral fit method. We are grateful to Ron Teclaw and Aaron Berger of the Rhinelander, Wisconsin, office of the U.S. Department of Agriculture Forest Service (USDAFS) for their assistance in maintaining the tower instrumentation. We also thank William Massman at the USDAFS Rocky Mountain Research Station, and the reviewers, for help with the phase formulation. We express gratitude to the State of Wisconsin Educational Communications Board and Roger Strand (chief engineer for WLEF-TV). The carbon dioxide mixing ratio measurements and site infrastructure and maintenance were supported by the Atmospheric Chemistry Project of the Climate and Global Change Program of the National Oceanic and Atmospheric Administration.

REFERENCES

Bakwin, P. S., P. P. Tans, D. F. Hurst, and C. Zhao, 1998: Measurements of carbon dioxide on very tall towers: Results of the NOAA/CMDL program. *Tellus,* **50B,** 401–415.

Baldocchi, D. D., S. B. Verma, and D. E. Anderson, 1987: Canopy photosynthesis and water-use efficiency in a deciduous forest. *J. Appl. Ecol.,* **24,** 251–260.

——, B. B. Hicks, and T. P. Meyers, 1988: Measuring biosphere–atmosphere exchanges of biologically related gases with micrometeorological methods. *Ecology,* **69,** 1331–1340.

Ciais, P., P. P. Tans, M. Trolier, J. W. C. White, and R. J. Francey, 1995a: A large Northern Hemisphere terrestrial CO_2 sink indicated by the $^{13}C/^{12}C$ ratio of atmospheric CO_2. *Science,* **269,** 1098–1102.

——, and Coauthors, 1995b: Partitioning of ocean and land uptake of CO_2 as inferred by $\delta^{13}C$ measurements from the NOAA Climate Monitoring and Diagnostics Laboratory Global Air Sampling Network. *J. Geophys. Res.,* **100,** 5051–5070.

Conway, T. J., P. P. Tans, L. S. Waterman, K. W. Thoning, D. R. Kitzis, K. A. Masarie, and N. Zhang, 1994: Evidence for interannual variability of the carbon cycle from the National Oceanic and Atmospheric Administration/Climate Monitoring and Diagnostics Laboratory Global Air Sampling Network. *J. Geophys. Res.,* **99,** 22 831–22 855.

Davis, K. J., P. S. Bakwin, C. Zhao, W. M. Angevine, D. F. Hurst, and J. G. Isebrands, 1996: Monitoring regional forest–atmosphere exchanges of carbon dioxide. *Proc. 22d Conf. on Agricultural and Forest Meteorology,* Atlanta, GA, Amer. Meteor. Soc., 302–305.

——, N. Gamage, C. R. Hagelberg, C. Kiemle, and D. H. Lenschow, 2000: An objective method for deriving atmospheric structure from airborne lidar observations. *J. Atmos. Oceanic Technol.,* **17,** 1455–1468.

Denning, A. S., I. Y. Fung, and D. Randall, 1995: Latitudinal gradient of atmospheric CO_2 due to seasonal exchange with land biota. *Nature,* **376,** 240–243.

Desjardins, R. L., J. I. Macpherson, P. H. Schuepp, and F. Karanji, 1989: An evaluation of aircraft flux measurements of CO_2, water vapor, and sensible heat. *Bound.-Layer Meteor.,* **47,** 55–69.

Fan, S. M., S. C. Wofsy, P. S. Bakwin, D. J. Jacob, and D. R. Fitzjarrald, 1990: Atmosphere–biosphere exchange of CO_2 and O_3 in the central Amazon forest. *J. Geophys. Res.,* **95,** 16 851–16 864.

Francey, R. J., P. P. Tans, C. E. Allison, I. G. Enting, J. W. C. White, and M. Trolier, 1995: Changes in oceanic and terrestrial carbon uptake since 1982. *Nature,* **373,** 326–330.

Friehe, C. A., and Coauthors, 1991: Air–sea fluxes and surface layer turbulence around a sea surface temperature front. *J. Geophys. Res.,* **96,** 8593–8609.

Goulden, M. L., J. W. Munger, S.-M. Fan, B. C. Daube, and S. C. Wofsy, 1996a: Exchange of carbon dioxide by a deciduous forest: Response to interannual climate variability. *Science,* **271,** 1576–1578.

——, ——, ——, ——, and ——, 1996b: Measurements of carbon sequestration by long-term eddy covariance: Methods and a critical evaluation of accuracy. *Global Change Biol.,* **2,** 169–182.

Grace, J., and Coauthors, 1995: Carbon dioxide uptake by an undis-

turbed tropical rain forest in southwest Amazonia, 1992 to 1993. *Science*, **270,** 778–780.

Grelle, A., and A. Lindroth, 1996: Eddy-correlation system for long-term monitoring of fluxes of heat, water vapour and CO_2. *Global Change Biol.,* **2,** 297–307.

Hignett, P., 1992: Corrections to temperature measurements with a sonic anemometer. *Bound.-Layer Meteor.,* **61,** 175–187.

Keeling, R. F., S. C. Piper, and M. Heimann, 1996: Global and hemispheric CO_2 sinks deduced from changes in atmospheric O_2 concentration. *Nature,* **381,** 218–221.

Lenschow, D. H., and B. B. Stankov, 1986: Length scales in the convective boundary layer. *J. Atmos. Sci.,* **43,** 1198–1209.

——, and M. R. Raupach, 1991: The attenuation of fluctuations in scalar concentrations through sampling tubes. *J. Geophys. Res.*, **96,** 15 259–15 268.

Leuning, R., and J. Moncrieff, 1990: Eddy-covariance CO_2 flux measurements using open-and closed-path CO_2 analyzers: Corrections for analyser water vapour sensitivity and damping of fluctuations in air sampling tubes. *Bound.-Layer Meteor.,* **53,** 63–76.

——, and K. M. King, 1992: Comparison of eddy-covariance measurements of CO_2 fluxes by open- and closed-path CO_2 analysers. *Bound.-Layer Meteor.,* **59,** 297—311.

Li-Cor, Incorporated, 1996: LI-6262 CO_2/H_2O analyzer operating and service manual. Publication 9003-59, Lincoln, NE, 100 pp. [Available from Li-Cor, Inc., Environmental Division, P. O. Box 4425, Lincoln, NE 68504.]

Massman, W. J., 1991: The attenuation of concentration fluctuations in turbulent flow through a tube. *J. Geophys. Res.,* **96,** 15 269–15 273.

McMillen, R. T., 1988: Eddy correlation technique with extended applicability to nonsimple terrain. *Bound.-Layer Meteor.,* **43,** 231–245.

Moncrieff, J. B., Y. Malhi, and R. Leuning, 1996: The propagation of errors in long-term measurements of land–atmosphere fluxes of carbon and water. *Global Change Biol.,* **2,** 231–240.

Moore, C. J., 1986: Frequency response corrections for eddy correlation systems. *Bound.-Layer Meteor.,* **37,** 17–35.

Ohtaki, E., 1985: On the similarity in atmospheric fluctuations of carbon dioxide, water vapor and temperature over vegetated fields. *Bound.-Layer Meteor.,* **32,** 25–37.

Philip, J. R., 1963: The theory of dispersal during laminar flow in tubes. II. *Aust. J. Phys.,* **16,** 300–310.

Shaw, W. J., C. W. Spicer, and D. V. Kenny, 1998: Eddy correlation fluxes of trace gases using a tandem mass spectrometer. *Atmos. Environ.,* **32,** 2887–2898.

Tans, P. P., I. Y. Fung, and T. Takahashi, 1990: Observational constraints on the global atmospheric CO_2 budget. *Science,* **247,** 1431–1438.

Taylor, G. I., 1953: Dispersion of soluble matter in solvent flowing slowly through a tube. *Proc. Roy. Soc. London Ser., A,* **219,** 186–203.

——, 1954: The dispersion of matter in turbulent flow through a pipe. *Proc. Roy. Soc. London Ser., A,* **223,** 446–468.

Wallace, J. M., and P. V. Hobbs, 1977: *Atmospheric Science: An Introductory Survey.* Academic Press, 467 pp.

Webb, E. K., G. I. Pearman, and R. Leuning, 1980: Correction of flux measurements for density effects due to heat and water vapour transfer. *Quart. J. Roy. Meteor. Soc.,* **106,** 85–100.

Wofsy, S. C., M. L. Goulden, J. W. Munger, S.-M. Fan, P. S. Bakwin, B. C. Daube, S. L. Bassow, and F. A. Bazzaz, 1993: Net exchange of CO_2 in a mid-latitude forest. *Science,* **260,** 1314–1317.

Yi, C., K. J. Davis, P. S. Bakwin, B. W. Berger, and L. C. Marr, 2000: The influence of advection on measurements of the net ecosystem–atmosphere exchange of CO_2 from a very tall tower. *J. Geophys. Res.,* **105,** 9991–9999.

Zhao, C. L., P. S. Bakwin, and P. P. Tans, 1997: A design for unattended monitoring of carbon dioxide on a very tall tower. *J. Atmos. Oceanic Technol.,* **14,** 1139–1145.